TABLE A1. VALUES OF $h(\lambda)$ AND $g(\lambda)$ FOR $\beta = 0.6$, $\alpha = 0.11$

R	λ	$h(\lambda)$	$g(\lambda)$
1	1.19	3.46	1.18
2	1.56	3.75	1.14
5	2.08	4.16	1.10
10	2.44	4.44	1.07
20	2.70	4.65	1.05
∞	3.03	4.91	1.03

Multiplying Eqs. A2, A3 and A4 and retaining only first-order terms, one finds for $\beta = 0.6$ that

$$f(l_g)(l_m/l_b)^{5/3}\left(1+\frac{\Delta_2}{\Delta_1}\right) \sim h_1(\lambda)(1+\epsilon g(\lambda)) \qquad \text{(A5)}$$

where $g(\lambda) = 1.35\,(1 + 0.16\lambda)/(1 + 0.31\lambda)$, $h_1(\lambda) = 0.79 + 0.245\lambda$ and $\lambda = (\alpha + \beta/R)^{-1/2}$, Table A1. Since Eq. A5 represents the first-order expansion of the power law $h_1(\lambda)(l_m/l_b)^{g(\lambda)}$, as $l_m/l_b \rightarrow 1$ and $(12/\beta^2)^{1/3} = 3.22$, Eq. A1 reduces to the simple form

$$\frac{[AB]}{[A]}\frac{u_o\gamma\,[B]_0}{kl_b} \sim h(\lambda)(l_m/l_b)^{g(\lambda)} \qquad \text{(A6)}$$

where $h(\lambda) = 2.53\,(1 + 0.31\lambda)$.

LITERATURE CITED

Brodkey, R. S., Ed., *Turbulence in Mixing Operations*, Academic Press (1975).

Escudier, M. P., "Aerodynamics of a Burning Turbulent Gas Jet in a Crossflow," *Comb. Sci. and Tech.*, **4**, 293 (1972).

Fay, J. A., "Buoyant Plumes and Wakes," *Ann. Rev. Fluid Mechanics*, **5**, 151 (1973).

Fischer, H. B., E. J. List, R. C. Y. Koh, J. Imberger, and N. H. Brooks, *Mixing in Inland and Coastal Waters*, 346, Academic Press (1979).

Forney, L. J., "Turbulent Plume in a Laminar Crossflow," MS Thesis, MIT, Cambridge, MA (1968).

Forney, L. J., and D. A. Heffner, "Slow Second Order Reactions in a Power Plant Plume: Application to Preliminary Data," *Chem. Engr. Comm.* **17**, 227 (1982).

Forney, L. J., and T. C. Kwon, "Efficient Single-Jet Mixing in Turbulent Tube Flow," *AIChE J.*, **25**, 623 (1979).

Forney, L. J., and Z. G. Giz, "Slow Chemical Reactions in Power Plant Plumes: Application to Sulfates," *Atoms. Envir.*, **14**, 533 (1980).

Forney, L. J., and Z. G. Giz, "Fast Reversible Reactions in Power Plant Plumes: Application to the Nitrogen Dioxide Photolytic Cycle," *Atmos. Envir.*, **15**, 345 (1981).

Freiberg, J., "Conversion Limit and Characteristic Time of SO_2 Oxidation in Plumes," *Atmos. Envir.*, **12**, 339 (1978).

Gouldin, F. C., "Role of Turbulent Fluctuations in NO Formations," *Comb. Sci. Tech.*, **9**, 17 (1974).

Heffner, D. A., "Analytical Expressions for Slow Pseudosecond-Order Reactions in Plumes: Comparison with Experimental Results," MS Thesis, Georgia Institute of Technology, Atlanta (1981).

Hoult, D. P., and J. A. Fay, and L. J. Forney, "A Theory of Plume Rise Compared with Field Observations," *J. Air Pollut. Control. Assoc.*, **19**, 585 (1969).

Hoult, D. P., and J. C. Weil, "Turbulent Plume in a Laminar Crossflow, *Atmos. Envir.*, **6**, 513 (1972).

Lin, C. H., and E. E. O'Brien, "Turbulent Shear Flow Mixing and Rapid Chemical Reactions: an Analogy," *J. Fluid Mech.*, **64**, 195 (1974).

McKelvey, K. N., H. N. Yieh, S. Zakanycz, and R. S. Brodkey, "Turbulent Motion, Mixing, and Kinetics in a Chemical Reactor Configuration," *AIChE J.*, **21**, 1165 (1975).

Morton, B. R., G. I. Taylor, and J. S. Turner, "Turbulent Gravitational Convection from Maintained and Instantaneous Sources," *Proc. Roy. Soc., London*, **A234**, 1 (1956).

Oakes, L. A., "Measurements of Slow Second-Order Reactions in a Buoyant Jet in a Crossflow," Tech. Rep. MSCEGT81-024, Georgia Institute of Technology, Atlanta (1981).

Rajaratnam, N., *Turbulent Jets*, Elsevier Scientific Pub. Co. (1976).

Schwartz, S. E., and L. Newman, "Processes Limiting Oxidation of Sulfur Dioxide in Stack Plumes," *Envir. Sci. Technol.*, **12**, 67 (1978).

Singh, M., and H. L. Toor, "Characteristics of jet mixers—effect of number of jets and Reynolds numbers," *AIChE J.*, **20**, 1224 (1974).

Torr, H. L., "The Nonpremixed Reaction: A + B → Products, Chap. 3," *Turbulence in Mixing Operations*, Ed., R. S. Brodkey, Academic Press (1975).

Wright, S. J., "Effects of Ambient Crossflows and Density Stratification on the Characteristic Behavior of Round Turbulent Buoyant Jets," Tech. Rep. KH-R-36, W. M. Keck Lab. of Hydroaulics, California Institute of Technology, Pasadena (1977).

Manuscript received January 25, 1982; revision received January 28, 1983, and accepted February 9, 1983.

Bubble Formation at Vibrated Orifices: Medium-Chamber-Volume Region

The bubble formation process at small, single, circular orifices at low gas flow rates is modified when the system is vertically vibrated in a sinusoidal fashion.

For systems with significant gas chamber volume, bubble volume in the vibrated case is smaller than in the nonvibrated case. The vibrations increase the amount of liquid weeping through the orifice into the gas chamber. A simple inviscid model adequately predicts bubble formation in the medium-chamber-volume region at low values of amplitude and frequency of vibration and low viscosities. The boundaries of the transition from the $FR \gg 1$ to the $FR = 1$ regions are described in terms of "the acceleration number/Eötvös number."

C. T. BAKER and NOEL de NEVERS

Department of Chemical Engineering
University of Utah
Salt Lake City, UT 84112

SCOPE

Bubbles play a significant role in many important industrial processes, including distillation, gas-liquid chemical reactors, absorption, and flotation. In many of these processes, bubbles are formed by forcing gas through an orifice into a liquid; the principal reason for doing this is to increase the interfacial area between gas and liquid.

The formation of bubbles at single, submerged orifices has

C. T. Baker is presently with Conoco, Ponca City, OK 74603.
Correspondence concerning this paper should be directed to N. de Nevers.

been extensively studied. To the knowledge of the authors, none of these previous studies has included the effects of vertical system oscillations on bubble formation.

When vertical oscillations are present in the bubble-forming system, the experimental bubble sizes are quite different from those observed in nonvibrating systems. Chemical plants and oil refineries are noisy operations. Vibrations are introduced from various sources into these facilities. Because vibrations play a significant role in bubble-forming phenomena, the results of this investigation bear directly on the analysis of these operations and help to indicate the range of applicability of previous analyses which have tacitly assumed the absence of such vibrations.

Previous mass transfer studies (Ruckenstein and Muntean, 1970; Lemcoff and Jameson, 1975) have shown that vertical sinusoidal oscillations increase the rate of mass transfer between bubbles and liquid. These studies do not include the effects of vibrations during bubble formation.

CONCLUSIONS AND SIGNIFICANCE

The effect of vertical vibrations on the volume of bubbles formed at a single, circular, horizontal orifice in an inviscid liquid can be accurately predicted with a simple mathematical model for low values of the acceleration number ($a\omega^2/g$). The vibrations generally reduce the bubble volumes, compared to the nonvibrated case.

At high values of the acceleration number, the bubble formation frequency becomes the same as the vibration frequency. Bubble volumes under these conditions are small, but the liquid weeping rate through the orifice between bubble formation cycles can exceed the inflowing gas supply rate by an order of magnitude.

Between these high and low values of the acceleration number, there exists a transition zone of irregular behavior whose boundaries are values of 1 and 2.6 of the dimensionless group (acceleration number/Eötvös number).

Some data were obtained for viscous liquids, showing that weeping did not occur and that average rather than instantaneous interface stability governs bubble release.

The significance of this work is that a simple mathematical model can predict bubble formation behavior in the region of greatest industrial interest. The boundaries of that region are calculable. The behavior at regions of high acceleration number and higher viscosity is partly elucidated by the results shown here.

This paper discusses the effect of vertical, sinusoidal vibrations on the bubble formation process for low gas flow rates and the medium range of gas chamber (plenum) volumes. This is an extension of the nonvibrated research described in detail by Park et al. (1977). There appears to be no previous work on the vibrated extension of this chamber volume region.

THEORY

Figure 1 shows an open liquid chamber, positioned above a closed gas chamber; a circular hole in the plate separating the two chambers allows gas flow for bubble formation. A gas is added to the lower chamber at a constant rate. The entire system is mounted on a table which moves vertically up and down at some preset amplitude and frequency.

Park et al. (1977) showed that for the system shown in Figure 1, without vibrations, the bubble-forming behavior takes on three different forms, depending on the size of the gas chamber or plenum below the orifice. This entire paper concerns the "medium chamber region," as they defined this term.

As discussed by Park et al. (1977), bubble formation takes place in two stages, chamber pressurization and chamber depressurization. The pressure in the lower chamber oscillates, rising and falling once per bubble, but has no long-term trend. For nonvibrated cases the pressurization step takes much longer than the depressurization step; typically the pressurization takes 99% of one formation cycle.

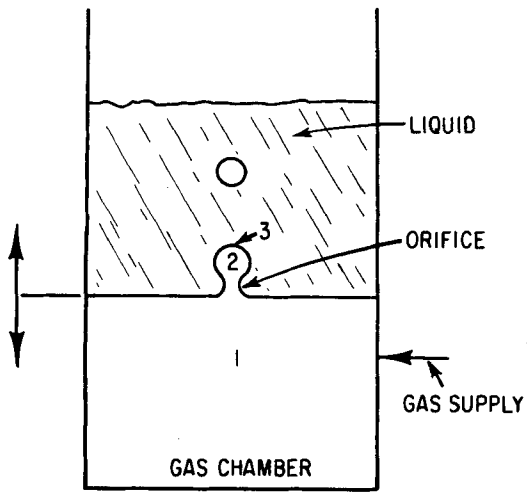

Figure 1. Schematic of bubble formation at an orifice with significant chamber volume.

The subscripts 1, 2 and 3 in the following equations refer to the gas chamber, the interior of the bubble, and the liquid directly above the gas-liquid interface, respectively (Figure 1).

The insertion of a chamber between the constant-flow-rate gas supply and the forming bubble allows the flow rate into the bubble to vary drastically with time, even with a constant flow rate from the gas supply system. The gas flow rate into the chamber remains essentially constant, but the flow rate out of the chamber is cyclical. The bubble emerges and releases above the orifice during a relatively small fraction of the cycle. The rest of the cycle consists of pressurization of the chamber to a value at which the bubble interface moves beyond the stable hemispherical stage.

The depressurization phase is that portion of the cycle during which the bubble expands into the liquid. In the vibrated case, the depressurization phase includes all events between the time when the bubble begins to expand and the time the bubble releases. The chamber pressure may rise during this phase due to gas flow back into the chamber. The rest of the formation cycle consists of rebuilding the chamber pressure to the value at which depressurization begins again.

During the pressurization phase, there is negligible gas flow out of the orifice or chamber, the pressure is increased by the gas flowing into the chamber from the supply system,

$$P_1 = P_{c0} + \frac{P_{\text{avg}} q_i (t - t_0)}{V_c} \tag{1}$$

The pressure at a depth h in a liquid undergoing vertical rigid-body oscillations (neglecting compressibility, standing waves, sloshing, etc.) is given by

$$P_3 = \rho_l h(g - a\omega^2 \cos\omega t) + P_0. \tag{2}$$

The gas-liquid interface in the orifice can accommodate small differences in pressure across it by changing its radius of curvature,

$$P_1 - P_3 = \frac{2\sigma}{R_i} \tag{3}$$

but this accommodation is limited by the minimum value of R_i, namely R_o. When the pressure difference exceeds $2\sigma/R_o$, the interface becomes unstable, the pressurization phase ends, and rapid bubble growth begins.

For small gas flow rates into the chamber (small rate of change of R_i) this transition should always occur at the top of an oscillatory cycle, when P_3 assumes its smallest value.

All other things being equal, an increase in acceleration number should result in a decrease in the maximum value of P_1, because the pressurization phase ends whenever

$$P_1 \geq \frac{2\sigma}{R_o} + g\rho_l h(1 - a\omega^2/g) + P_o. \tag{4}$$

The above discussion ignores viscous resistance to the expanding interface. In a previous paper on the zero-chamber-volume region (Barker and de Nevers, 1982), it was shown that, when viscous forces become significant compared to inertial forces, instantaneous instability is not enough to trigger bubble release. The transition will occur only when the interface is unstable for a significant fraction of the vibratory cycle. For viscous liquids, the maximum chamber pressure will be independent of acceleration ratio.

During the depressurization phase, the flow rate out of the chamber through the orifice is much greater than the flow rate into the chamber from the supply system. For practically constant temperature, constant gas density and ideal gases, a mass balance on the chamber yields

$$\frac{dP_1}{dt} = \frac{P_{avg}}{V_c}(q_i - \pi R_0^2 \mathcal{V}_2) \tag{5}$$

The rate of change of bubble volume is given by

$$\frac{dV_b}{dt} = \pi R_0^2 \mathcal{V}_2 \tag{6}$$

The pressure within the bubble (P_2), is calculated from

$$P_2 = P_o + \rho_l h(g - a\omega^2 \cos\omega t) + \frac{2\sigma}{R_i} \tag{7}$$

which assumes that the pressure in the bubble is in equilibrium with the instantaneous liquid pressure at the depth of the orifice. This is equivalent to assuming that the pressure differences due to inertial and viscous effects at the surface of the growing bubble are negligible compared to the inertial pressure drop through the orifice. A single, spherical radius of curvature is assumed to be an adequate substitute for the two perpendicular radii of curvature whose average should appear in Eq. 7.

The velocity of gas flow through the orifice is calculated by Bernoulli's equation using the P_1 from Eq. 5 and P_2 from Eq. 7, and an orifice coefficient of 0.65 (Tuve and Sprenkle, 1933). This coefficient is the only experimental value used in the model; there are no adjustable parameters.

This simple model is a direct extension of the model described by Park et al. (1977) for the nonvibrated case and has the satisfactory property that it matches their results as the vibrations become negligible.

Equations 5, 6 and 7, and Bernoulli's equation form a set of ordinary differential equation (ODE's) which can be solved for a suitable initial condition. Equation 4 provides a suitable initial pressure, together with an initial volume equal to a hemisphere of radius R_o, and an initial time corresponding to the top of the vibratory cycle. This ODE problem was solved for a large variety of conditions, using the methods of C. W. Gear, as implemented in the IMSL Library at The University of Utah Computer Center. The program is listed in Barker (1981).

The integration was terminated and bubble release reported when the following two conditions were simultaneously satisfied: $P_1 - P_2 < \epsilon$, where ϵ is a small value, and $F_b > 2\sigma/R_o$. These indicate that release occurs when the flow rate into the bubble has become negligible and simultaneously the buoyant force (which is itself oscillatory at a fixed bubble volume due to external pressure oscillations) is greater than the surface force holding the bubble to the orifice.

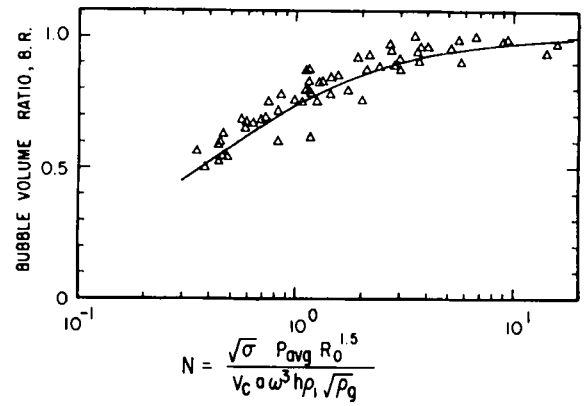

Figure 2. Bubble volume ratio for the medium chamber region with inviscid liquids and $FR \gg 1$.

The calculated bubble volumes are functions of system geometry, fluid properties, and vibration parameters. They do not appear to be reducible to any simple analytic equation. The most compact representation found for them is the solid line on Figure 2. (The triangles represent experimental data discussed later.) The plot shows the ratio of predicted bubble volume under vibrated conditions to predicted bubble volume for identical system geometry, fluid properties, and gas flow rate without vibrations, as a function of a dimensionless group, N. This latter group may be factored into three dimensionless parts,

$$N = \frac{\sqrt{\sigma}\, P_{avg} R_o^{1.5}}{V_c a\omega^3 h \rho_l \sqrt{\rho_g}} = \frac{g}{a\omega^2} \times \frac{\sigma}{g\rho_l R_o h} \times \frac{R_o^{5/2} P_{avg}}{\sqrt{\sigma\rho_g} V_c \omega} \tag{8}$$

The first part is the reciprocal of the acceleration number, the ratio of the peak vibrational acceleration to the gravitational acceleration. The second part is an Eötvös number, the ratio of surface to gravitational forces in the liquid. Here the L^2 in the Eötvös number is taken in two perpendicular directions, h and R_o. The third part has no common name nor such a simple interpretation. It is arrived at by reasoning that

$$V_b = \pi R_o^2 \int_0^t \mathcal{V}_2 dt \cong \pi R_o^2 \mathcal{V}_{\text{initial}} \cdot \Delta t \tag{9}$$

The time of bubble formation is about half a vibrational cycle, so Δt is replaced with π/ω. The initial velocity through the orifice is given by

$$\mathcal{V}_{\text{initial}} = C_v \sqrt{\frac{2\Delta P}{\rho_g}} = C_v \sqrt{\frac{2\sigma}{R_o \rho_g}} \tag{10}$$

and

$$V_b = C_v \frac{\pi^2 R_o^2}{\omega} \sqrt{\frac{2\sigma}{R_o \rho_g}} \tag{11}$$

Taking the ratio of this bubble size to that formed in the medium chamber region without vibrations (Park et al., 1977),

$$V_{\text{nonvibrated}} = \frac{2\sigma V_c}{K R_o P_{avg}} \tag{12}$$

leads to

$$\frac{V_b}{V_{\text{nonvibrated}}} \cong \text{some constant} \frac{R_o^{5/2} P_{avg}}{\sqrt{\sigma\rho_g} V_c \omega} \tag{13}$$

This logic shows whence the rightmost dimensionless group in Eq. 8 comes and suggests that it alone would be a suitable correlating parameter. But comparison of a large number of computed bubble volumes with varying input parameters showed that the product of three dimensionless groups making up N in Eq. 8 is a far superior correlating parameter. The solid line shown on Figure 2 represents

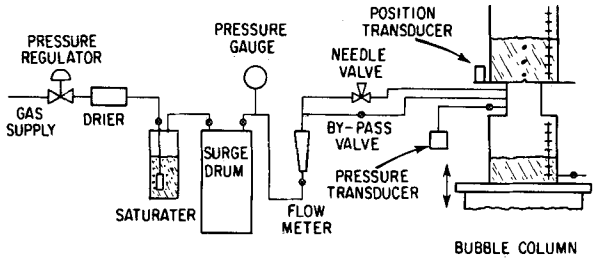

Figure 3. Schematic of equipment used for tests with significant chamber volume below the orifice plate.

all the computed bubble volumes ratios in this region with an average error of 1.2%.

This model is only appropriate for the region in which

$$\text{Frequency Ratio } (FR) = \frac{\text{No. of vibrational cycles}}{\text{No. of bubbles formed}} \qquad (14)$$

is significantly greater than one and for low-viscosity fluids.

For the other regions of observed behavior, the theory is more explanation of observations than model building; it is presented with the experimental results.

Other workers in the formation of bubbles (Kumar and Kuloor, 1970; McCann and Prince, 1969; Marmur and Rubin, 1976; La-Nauze and Harris, 1974) have presented no theory directly applicable to this type of problem. The computer algorithms for predicting the bubble shape during the growth process of Pinczewski (1981) and Marmur and Rubin (1976) should be extendable to the vibrated case; that is being attempted in the continuation of this work.

APPARATUS AND PROCEDURE

Figure 3 represents the arrangement of equipment for these tests. The pressure regulator, drier, saturater, and surge drum were used to feed a constant supply of gas, saturated with vapor from the liquid into which the bubbles have formed, at 34.5 kPa, to the upstream side of the needle valve. The flowmeter was used to establish an approximate gas flow rate with the needle valve. The by-pass valve was used to help in resetting the liquid level in the gas chamber between runs when weeping occurred. The bubble column was identical to that described by Park et al. (1977) with the exception of the position transducer and a baffle plate on top of the upper chamber.

The bubble chamber was mounted on a vibratory table (All American Machine Co., Model 100VA) which caused the entire apparatus to move up and down in a sinusoidal motion, with externally controlled frequency and amplitude.

A steady-state gas flow was established without vibrations, and measured with a soap-film flowmeter. Then the vibrator was started, and its frequency, amplitude and phase were determined with a linear-voltage differential-transformer-type transducer and indicator (Boulton Paul Aircraft Ltd., Type EP 597). The bubble frequency and gas chamber pressure were measured by interpretation of the output from a differential pressure transducer (Pace Engineering, Model P7D) and indicator (Pace Engineering, Model CD25) connected to the gas chamber. The pressure changes in the gas chamber are related to the bubble formation sequence as discussed in the nonvibrated case by Park et al. (1977).

The electrical signals from the two transducers were digitally recorded for analysis with a Tektronix 4051 computer and a TransEra Model 652-ADC Analog-to-Digital converter.

Visual observations of the formation process were made with the strobe light. A photoelectric pickoff (General Radio, Type 1536-A) and flash delay (General Radio, Type 1531-P2) made it possible to view in repeated fashion all events at any position of the vibratory cycle by darkening the room and directing the flash at the orifice. The visual observations during runs helped interpret the recorded signals from the transducers in terms of the formation process. Table 1 presents the parameter ranges tested in this region.

TABLE 1. RANGE OF PARAMETERS FOR EXPERIMENTAL TESTS

Parameter	Minimum	Maximum
D_o, mm	1.21	3.875
ρ_l, kg/m^3	0.773×10^3	1.25×10^3
μ, Pa·s	0.878×10^{-3}	0.4802
σ, N/m	0.0228	0.0688
a, mm	0	1.59
f, Hz	6	40
h, mm	25.4	50.8
q_i, mm^3/s	40	70
$a\omega^2/g$	0	$\cong 7$

RESULTS AND DISCUSSION

Within the medium chamber volume region for inviscid fluids, bubble volume data as a function of vibrational frequency (holding all other parameters constant) typically yield plots such as that shown in Figure 4. The bubbles formed at low acceleration numbers are uniform in size; the volume decreases with increasing acceleration number. The pressurization phase takes many vibrational cycles ($FR \gg 1$). Bubbles formed in the transition region are not uniform in size; their sizes do not appear to follow any repeating sequence. At high acceleration numbers, the bubbles formed are of uniform size with one bubble formed on each vibrational cycle.

This discussion of results for the medium chamber region is divided into four parts.

$FR \gg 1$, Inviscid Liquids

For all experimental data which belong to this category, the mathematical model described above predicted bubble volume ratio as a function of all parameters within an average of 6.5% of the experimental value (maximum error of 25.5%).

Figure 2 shows this agreement between the experimental data points (shown as triangles) and the model.

Maximum chamber pressure in this region is in fair agreement with the theory. Figure 5 presents the experimental data for maximum chamber pressure as a function of the acceleration number. The solid line is Eq. 4. The average error, computed as (observed-calculated/observed), is 5.3%; the maximum error is 15.4%.

For most experimental conditions in this region, weeping did not occur. Figure 6 shows experimental weeping rates for some of the conditions in which it did. It appears from the figure that the weeping rate increases with acceleration number except in the case of the 60% glycerol-in-water solution. The opposite behavior is due to the viscosity of the liquid which is an order of magnitude larger than that of the other liquids shown on this figure.

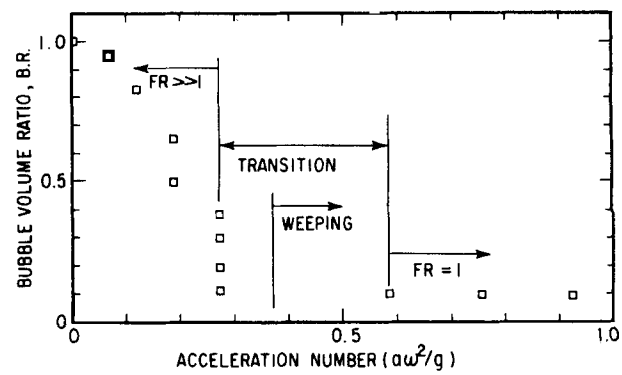

Figure 4. Typical plot of bubble volume ratio as a function of acceleration number for inviscid liquids.

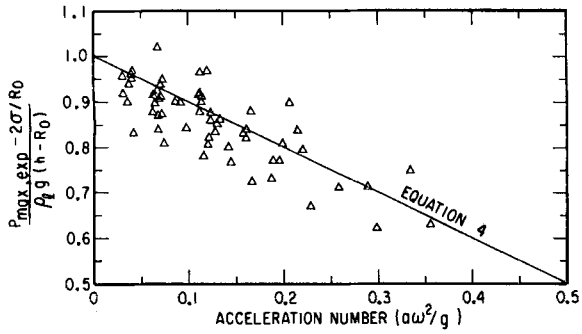

Figure 5. Experimental maximum chamber pressure as a function of acceleration number in the medium chamber region for the inviscid fluids and *FR* ≫ 1.

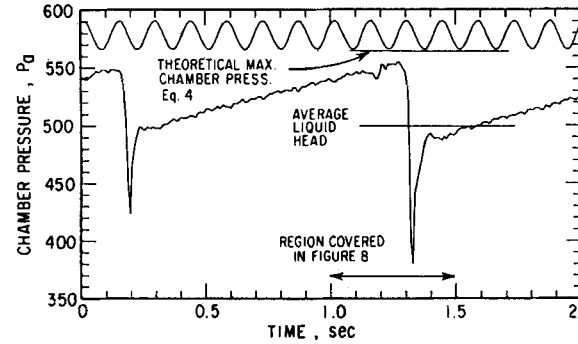

Figure 7. Chamber pressure history for bubble formation in the medium chamber region, inviscid liquids, *FR* ≫ 1. The curve at the top of the figure show the table position, as an indication of where in the cycle events occur.

Apparently this viscosity dependence of weeping for high-viscosity fluids is the same phenomenon previously observed in bubble formation; when the viscosity is high, the interface between gas and liquid must be unstable over a large part (or all) of the vibratory cycle for flow to occur. With low-viscosity liquids it need only be unstable over some small part of the cycle for the flow to occur.

From the inviscid data one may generalize that weeping in this region increases with increases in orifice diameter, acceleration ratio, chamber volume, and liquid head, and with a decrease in surface tension.

The gas chamber pressure history typical of this region (in a case with liquid weeping) is shown in Figures 7 and 8. Figure 7 shows most of two complete cycles; Figure 8 has an expanded time scale, showing only part of the bubble release shown in Figure 7. In both of these figures, the sine curve at the top shows the table position, indicating where in the vibratory cycle the events occur. Figure 7 shows the maximum expected pressure, from Eq. 4, as well as the average liquid pressure over the cycle. Figure 8 shows the predicted liquid head at the bottom of the vibratory cycle, given by

$$P_{3_{max}} = \rho_l h(1 + a\omega^2), \qquad (15)$$

as well as the magnitude of the maximum pressure difference due to surface tension ($2\sigma/R_o$) and the value of 69 Pa.

Pressurization of the gas chamber takes place prior to point A. Depressurization begins at the top of the vibratory cycle where the instantaneous liquid pressure is lowest. Depressurization and the corresponding bubble expansion takes place between points A and B.

The data shown on Figure 8 were logged at a rate of 128 values/second. It is possible that the true minimum chamber pressure occurred between digitized points and that the true minimum occurs just prior to point B. Between points B and C, several events occur. The bubble neck becomes smaller and the bubble accelerates upwards, which results in bubble release. At the same time a small amount of gas which is left behind in the neck flows back into the chamber, causing a sharp pressure rise. As the liquid begins to follow this gas downward through the orifice, the rate of pressure rise drops suddenly, at point C.

This change in pressure rise rate is due to a change in fluid flow rate. For comparable pressure-difference driving force, Bernoulli's equation for an orifice shows that the velocity is proportional to $(\rho^{-0.5})$. The liquid density is roughly a thousand times that of the gas; hence we would expect a roughly 30-fold decrease in the rate of pressure rise, as observed.

Liquid weeping continues to point D where the pressure in the gas chamber is high enough to stop the liquid flow. It corresponds closely in time to the bottom of the vibratory cycle. The calculated liquid pressure at point D (Eq. 15) is 543.4 Pa. The maximum pressure rise due to a hemispherical drop below the orifice plate (Eq. 3) is −112.8 Pa. Thus the pressure in the chamber is high enough at the bottom of the cycle to stop liquid flow through the orifice, if a coherent gas-liquid interface has been established. Even at point C the combination of chamber pressure and surface tension force would be adequate to stop the liquid flow if such an interface had been established, and the liquid possessed no downward momentum. In nonweeping cases (which are the majority), that occurs; in this case, it does not.

The pressure-time trace for nonweeping cases (the most common in this region) is similar to and simpler than the trace shown in Figures 7 and 8. On a nonweeping pressure trace, the wiggly ramp function of rising pressure corresponding to the pressurization phase extrapolated downward directly to the nearly-vertical depressurization phase. There is a minor disturbance at their intersection, but not the downward spike observed in weeping cases, like Figures 7 and 8.

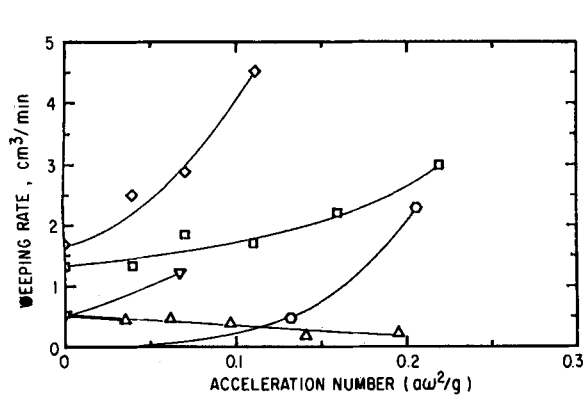

Figure 6. Weeping rate a a function of acceleration number for inviscid liquids and *FR* ≫ 1. Here △60% glycerol in water, D_o = 1.20 mm, h = 25.4 mm, a = 0.24 mm, V_c = 90 × 10⁻⁶m³; ▽water, D_o = 1.20 mm, h = 25.4 mm, a = 0.47 mm, V_c = 96; ○cyclohexane, D_o = 1.20 mm, h = 25.4 mm, a = 0.51 mm, V_c = 95; □cyclohexane, D_o = 1.20 mm, h = 25.4 mm, a = 0.27 mm, V_c = 49; ◇cyclohexane, D_o = 1.20 mm, h = 50.8 mm, a = 0.27 mm, V_c = 97

FR = 1, Inviscid Liquids

This region of bubble formation is characterized by the formation and release of one bubble during each vibrational cycle. Liquid

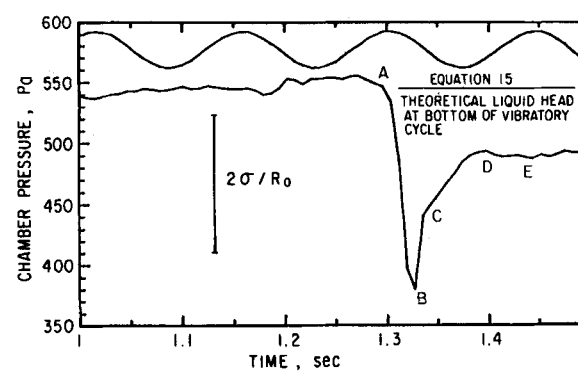

Figure 8. Expanded view of Figure 7.

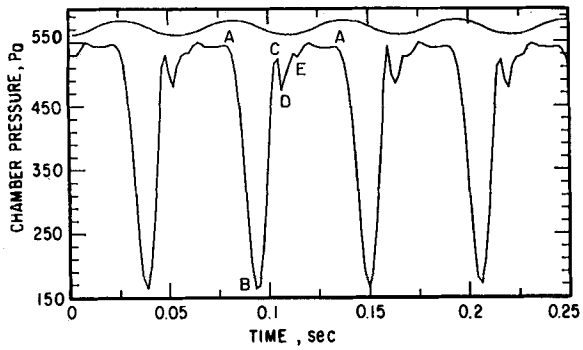

Figure 9. Typical chamber pressure history in the medium chamber region, inviscid liquids, $FR = 1$.

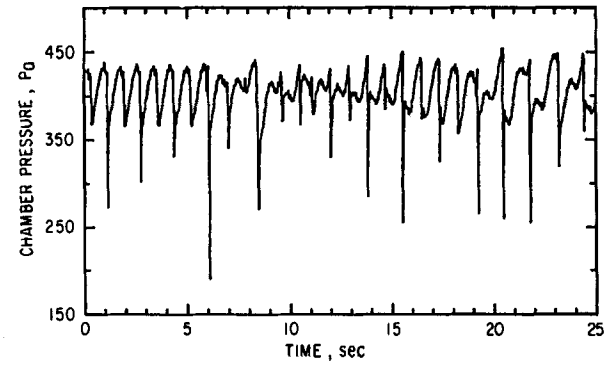

Figure 11. Typical chamber pressure history in the transition region, medium chamber, inviscid liquid.

weeping in this region is common to nearly all experimental tests. A typical chamber pressure history for four bubble cycles is shown in Figure 9. The time scale on Figure 9 is greatly expanded compared to Figures 7 and 8. One bubble forms every 0.056 s in Figure 9 compared to one every second in the previous figures. The acceleration number is 0.59 in Figure 9, compared to 0.09 in Figures 7 and 8.

The calculated maximum chamber pressure for a hemispherical interface at the top of the vibratory cycle (Eq. 4) in this case is 317.4 Pa. The experimental maximum pressure (550 Pa) is much higher than Eq. 4 predicts. Clearly, at this high acceleration number with resulting high liquid weeping velocities, the quasistatic assumptions leading to Eq. 4 are inappropriate. The relation between observed maximum chamber pressure and acceleration number is shown on Figure 10, in which

$$\frac{\%\ \text{Excess}}{\text{Max. Pres.}} = \frac{P_{\max,\exp} - P_{\max,\text{Eq.4}}}{P_{\max,\text{Eq.4}}} \times 100. \qquad (16)$$

Each bubble formation cycle, Figure 9, has several parts that can be related to physical events at the orifice. Point A was the beginning of depressurization which began slightly before the top of the vibratory cycle. The bubble interface began to expand upward into the liquid. Point B was the end of depressurization and the start of gas back-flow into the orifice. Between A and B the bubble expanded in a spherical shape. From B to C, the bubble shrank due to gas back-flow into the gas chamber and necked off at C. The gas was forced back into the chamber between B and C even though an equilibrium force balance predicted bubble release during most of the time between A and C.

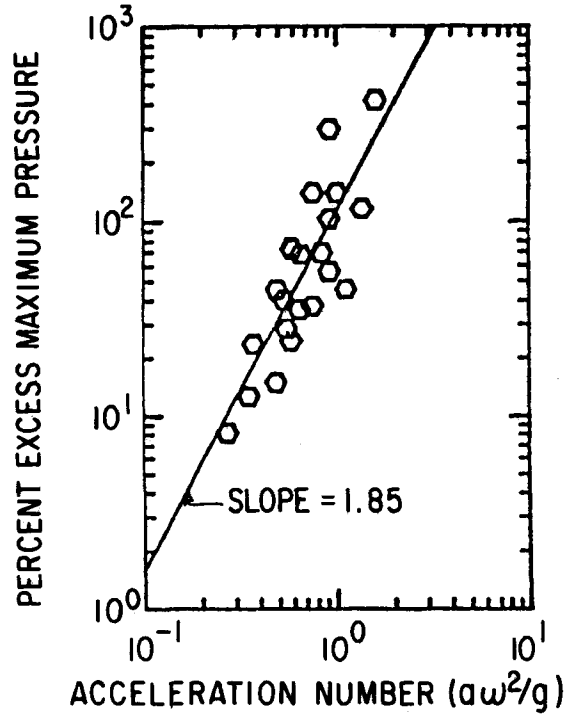

Figure 10. Percent excess maximum chamber pressure as a function of acceleration number, medium chamber region, inviscid liquids, $FR = 1$.

The model which serves well in the region of low acceleration numbers and much slower bubble formation is inapplicable here, because the viscous and inertial resistances to bubble motion, which were assumed negligible compared to the inertial resistance of gas flow through the orifice, are no longer negligible when the time scale for bubble formation and release is reduced (by a factor of 20 between Figures 8 and 9).

The shape of the bubble above the orifice plate between B and C was markedly different than that between A and B. The height of the bubble remained nearly constant while the sides of the bubble moved inward, forming a quasicylindrical column. The column necked off leaving a small bubble to rise to the surface. The pressure corresponding to C is nearly as high as at the beginning of depressurization. This is apparently due to the higher external liquid pressure at this point in the vibratory cycle (almost at the bottom). The drop in pressure from C to D, at a time when the external liquid pressure was still rising, was apparently caused by a change in the surface tension force, due to the rearrangement of the thin, practically cylindrical bubble into a close-to-spherical shape just before weeping began.

Weeping began at some point between C and D, and continued to E, at which point the interface reestablished itself. The pressure variations between E and the next A, which are fairly reproducible from cycle to cycle, have a higher frequency than the driving vibratory cycle. They presumably result from oscillatory movements of the gas-liquid interface. During this entire period, the interface is unstable with respect to upward motion; it apparently begins to move upward again at the next A when the external pressure has fallen far enough for the interface oscillations to grow into the fluid.

In this region, where the bubble frequency has "locked on" to the vibrational frequency, the weeping rate is the true determinant of bubble volume. The bubble volume is given by

$$V_b = \frac{q_i}{f} + \frac{q_w}{f}, \qquad (17)$$

In most cases, the righthand term has a value several times that of the left term.

Transition, Inviscid Liquids

This region of bubble formation, intermediate between the $FR \gg 1$ and the $FR = 1$ regions, was observed in every set of experimental runs. It is characterized by nonconstant consecutive bubble volume, with a wide range of volume values and no apparent pattern.

Figure 11 shows a typical chamber pressure history over about 35 bubble formation cycles. Here the trace of table position is not shown at the top of the figure because it would be a blur. At the leftmost part of the figure there were roughly seven vibratory cycles per bubble-formation cycle. Each of the major pressure

cycles shown here is a bubble formation cycle. Because the gas flow rate was constant, the size of a bubble was roughly proportional to the time between pressure peaks, except as complicated by weeping. At the left of the figure the first eight bubbles alternated regularly between nonweeping (as shown by pressure not falling below 350 Pa) and weeping bubbles in which the pressure fell much below this value, and was then returned by the inflow of liquid. To the right on the figure most bubbles had significant weeping, and a pattern of one very small bubble followed by one large bubble is apparent. For all the bubbles shown on this figure all of the external experimental conditions were held constant.

No model which assumes that each bubble is like its predecessor (or that the peculiarities of one bubble do not induce a different set of peculiarities in the next) can hope to explain the data in this region. However, it is possible to correlate the boundaries of this region. In the region of $FR \gg 1$ (to the left of Figure 4) the pressure difference due to surface tension (Eq. 3) is greater than the pressure swing due to vibration ($\rho_l h a \omega^2$). One would expect the transition to begin when these become roughly equal, and the lock-on of bubble formation frequency to vibration frequency ($FR = 1$ at the right of Figure 4) to occur when the pressure swing due to vibrations was significantly larger than the pressure difference due to surface tension. One may think of this transition as the region between a surface-tension-controlled situation to an inertially controlled one. The transition region is one in which both effects are significant. To test this hypothesis, the ratio of pressure swing due to vibration to maximum surface tension pressure

$$C_1 = \frac{2\rho_l h a \omega^2}{2\sigma/R_o} = \frac{\rho_l h a \omega^2 R_o}{\sigma} \tag{18}$$

was computed for all the experimental data. C_1 is the acceleration number, divided by the Eötvös number, Eq. 8. For all the cases examined, the value of C_1 at the onset of transition averaged 0.96 with a standard deviation of 0.19 while the value of C_1 at the end of transition averaged 2.63, with a standard deviation of 0.52. These values appear independent of whether the transition region was crossed by increasing or decreasing the vibratory frequency; there was no observed hysteresis.

Viscous Liquids

A few tests with a 96% glycerol-in-water solution revealed results quite different from the results for inviscid liquids. The most salient findings were that no weeping was encountered, even for acceleration numbers up to 0.57. The observed maximum pressures, and the bubble frequency ratios in the low acceleration number region were substantially unaffected by vibration. This is in accord with the conclusion for the zero-chamber volume region (Barker and de Nevers, 1982), that at high enough viscosities instantaneous interface instability is of no effect, and the stability averaged over the entire vibratory cycle is the controlling factor in bubble release. A region of $FR = 1$ was observed in which bubble volume decreased linearly with frequency, because no weeping was observed. But not enough data are available to form substantial conclusions.

CONCLUSIONS

$FR \gg 1$, Inviscid Liquids

The effect of vertical vibrations on bubble volume in this region is well predicted by a simple mathematical model that required the use of only one experimental constant, the orifice coefficient. The approximate upper boundary of this region is given by (acceleration No./Eötvös No.) = 1. The vibrations generally result in reduced bubble volume.

$FR = 1$, Inviscid Liquids

The approximate lower vibrational boundary for this region is (acceleration No./Eötvös No.) = 2.6. The bubble shape becomes cylindrical prior to bubble release. The bubble volume remained nearly constant while the weeping rate increased with increased vibrational frequency. The phenomena of gas flowback into the chamber were pronounced in this region.

Transition, Inviscid Liquids

A region of nonuniform bubble volume formation was always observed between the $FR \gg 1$ and $FR = 1.0$ regions. At fixed experimental conditions the bubble size and chamber pressure fluctuated without detectable periodicity. The region boundaries are independent of whether the region is crossed with increasing or decreasing frequency.

Viscous Liquids

Weeping was not observed even at an acceleration number of 0.5. Instantaneous interface instability does not appear to determine whether or not a bubble forms; the average of the forces over the entire vibrational cycle seems to be controlling.

ACKNOWLEDGMENTS

This work was supported by National Science Foundation Grant ENG-7909104.

NOTATION

a = amplitude of vibration, m
BR = bubble volume ratio ($V_b/V_{\text{nonvibrated}}$)
C_1 = acceleration No./Eötvös No. (Eq. 18)
c_v = orifice coefficient
f = frequency of vibration, Hz
D_o = orifice diameter, m
FR = frequency ratio (ratio of vibrational frequency to bubble formation frequency)
F_b = instantaneous buoyant force, N
g = gravitational acceleration constant, m/s^2
h = liquid head, m
K = polytropic coefficient, Eq. 12
N = dimensionless group in medium chamber region (Eq. 8)
P = pressure, Pa
P_o = system pressure, Pa
P_1 = chamber pressure, Pa
P_2 = interior bubble pressure, Pa
P_3 = pressure on liquid side of bubble interface, Pa
P_{avg} = average chamber pressure, Pa
P_{co} = initial chamber pressure, Pa
$P_{\max}$ = maximum chamber pressure during bubble cycle, Pa
$a\omega^2/g$ = acceleration number
q_i = gas flow rate, m^3/s
q_w = liquid (weeping) flow rate, m^3/s
R_i = instantaneous radius of curvature of bubble, m
R_o = orifice radius, m
t = time, s
t_o = initial time, s
V_c = chamber volume, m^3
V_b = bubble volume, m^3
$V_{\text{nonvibrated}}$ = experimental calculated bubble volume (Eq. 12), m^3
$\mathcal{V}_2$ = gas velocity in orifice, m/s
$\mathcal{V}_{\text{initial}}$ = initial gas velocity in orifice, m/s

Greek Letters

ϵ = small value of variable (varies)
$\Delta\rho$ = gas-liquid density difference, kg/m^3

ρ_g = gas density, kg/m^3
ρ_l = liquid density, kg/m^3
σ = surface tension, N/m
ω = radial velocity, rad/s
μ = viscosity, Pa·s

LITERATURE CITED

Barker, C. T., "Bubble Formation at Vibrated Orifices," Ph.D. Dissertation, Chemical Engineering, The University of Utah (1981) (Available through University Microfilms).

Barker, C. T., and N. de Nevers, "Bubble Formation in a Vertically Vibrated System—Tate's Law Region," *AIChE J.*, **28**, 85 (1982).

Kumar, R., and N. R. Kuloor, "The Formation of Bubbles and Drops," *Adv. in Chem. Eng.*, **8**, T. B. Drew et al., Eds., Academic Press, New York (1970).

LaNauze, R. D., and I. J. Harris, "Gas-Bubble Formation at Elevated-System Pressures," *Trans. Instn. Chem. Engrs.*, **52**, 337 (1974).

Lemcoff, N. O., and G. J. Jameson, "Solid Liquid Mass Transfer in a Resonant Bubble Contractor," *Chem. Eng. Sci.*, **30**, 363 (1975).

Marmur, A., and E. Rubin, "A Theoretical Model for Bubble Formation at an Orifice Submerged in an Inviscid Liquid," *Chem. Eng. Sci.*, **31**, 453 (1976).

McCann, D. J., and R. G. H. Prince, "Bubble Formation and Weeping at a Submerged Orifice," *Chem. Eng. Sci.*, **24**, 801 (1969).

Park, Y., A. L. Tyler, and N. de Nevers, "The Chamber Orifice Interaction in the Formation of Bubbles," *Chem. Eng. Sci.*, **32**, 907 (1977).

Pinczewski, W. V., "The Formation and Growth of Bubbles at a Submerged Orifice," *Chem. Eng. Sci.*, **36**, 405 (1981).

Ruckenstein, E., and O. Muntean, "Mass Transfer Between a Bubble and An Oscillating Liquid," *Chem. Eng. Sci.*, **25**, 1159 (1970).

Tuve, G. L., and R. E. Sprenkle, "Orifice Discharge Coefficients for Viscous Liquids," *Instruments*, **6**, 201 (1933).

Manuscript received April 7, 1982; revision received October 27, and accepted January 31, 1983.

Effects of Radially Nonuniform Distributions of Catalytic Activity on Performance of Spherical Catalyst Pellets

The performance of spherical catalyst pellets with radially nonuniform distributions of activity is simulated under parallel reaction networks closely resembling hydrocarbon oxidation reactions. Both reaction paths are assumed to be exothermic with the desired path exhibiting lower activation energy requirements than the undesired one. It is shown that nonuniform activity distributions enhance effectiveness and selectivity over a large range of values of the Thiele modulus. Multiple steady states in effectiveness and selectivity are observed for certain values of the heat of reaction parameter.

D. L. JOHNSON and X. E. VERYKIOS

Department of Chemical Engineering
Drexel University
Philadelphia, PA 19104

SCOPE

It is well known that significant concentration gradients develop within industrial catalyst particles due to increased diffusional resistances offered by the tortuous pore structure of the catalyst. Furthermore, if the reactions are sufficiently exothermic, significant intraparticle temperature gradients can also develop. These gradients alter not only the effectiveness of the catalyst in terms of its global rate, but also the selectivity in cases where multiple reactions of different order and/or activation energy occur. It has been shown (Becker and Wei, 1974, 1977a,b; Shadman Yazdi and Petersen, 1972; Corbett and Luss, 1974; Villadsen, 1976) that the distribution of catalytic activity within the catalyst particle can alter intrapellet concentration and temperature gradients which, in turn, can significantly influence the effectiveness and selectivity of the catalyst.

In the present study, the performance of spherical catalyst pellets with nonuniform activity distributions of the form: $K(r) = K_s(r/r_s)^\alpha$, $\alpha > 0$, is simulated under a parallel reaction network of the form: $A + B \rightarrow C + D$; $A + B \rightarrow E + F$. Reactions are assumed to exhibit second-order kinetics and to be exothermic. The desired reaction is of lower activation energy requirements than the undesired reaction. This reaction scheme, with the stated assumptions, very closely resembles catalytic hydrocarbon oxidation reactions. Intraparticle concentration and temperature profiles are obtained for various activity distributions by numerically solving the mass and energy diffusion equations. Effectiveness factors and overall pellet selectivities for various values of the dimensionless activation energies and heat of reaction parameters are then computed as a function of the Thiele modulus.

CONCLUSIONS AND SIGNIFICANCE

A mathematical simulation of the performance of spherical catalyst particles with radially nonuniform distribution of catalytic activity under parallel, exothermic reaction networks is presented. It is demonstrated that significant reduction of intraparticle concentration and temperature profiles results from nonuniform activity distributions. Effectiveness factors

D. L. Johnson is presently with the Paulsboro Laboratory, Paulsboro, NJ 08066.